Neurobiology of Disease 121 (2019) 95–105

Contents lists available at ScienceDirect

Neurobiology of Disease

journal homepage: www.elsevier.com/locate/ynbdi

TSPO and amyloid deposits in sub-regions of the hippocampus in the 3xTgAD mouse model of Alzheimer's disease

Benjamin B. Tournier[a], Stergios Tsartsalis[a], Daphney Rigaud[a], Christine Fossey[b], Thomas Cailly[b,c], Frédéric Fabis[b], Tien Pham[d], Marie-Claude Grégoire[d], Eniko Kövari[e,f], Marcelle Moulin-Sallanon[a,g], Armand Savioz[e], Philippe Millet[a,f,*]

[a] Division of Adult Psychiatry, Department of Mental Health and Psychiatry, University Hospitals of Geneva, Switzerland
[b] Normandie Univ, UNICAEN, CERMN, F-14032 Caen, France
[c] Department of Nuclear Medicine, CHU Cote de Nacre, 14000 Caen, France
[d] ANSTO LifeSciences, Australian Nuclear Science and Technology Organisation, New Illawarra Road, Sydney, NSW 2234, Australia
[e] Division of Geriatric Psychiatry, Department of Mental Health and Psychiatry, University Hospitals of Geneva, Switzerland
[f] Department of Psychiatry, University of Geneva, Switzerland
[g] INSERM Unit 1039, J. Fourier University, La Tronche, France

ARTICLE INFO

Keywords:
Neuroinflammation
Alzheimer's disease
TSPO
CLINDE
DRM106
3xTgAD

ABSTRACT

The involvement of the 18kDa translocator protein (TSPO), a marker of neuroinflammation, in Alzheimer's disease (AD) remains controversial. In the present report, we used [^{125}I]-CLINDE, a SPECT TSPO radiotracer never before used in AD, and we investigated the relationship between TSPO and amyloid plaque density (using [^{125}I]-DRM106) in a triple transgenic mouse model of AD (3xTgAD, APP_{SWE}, $PS1_{M146V}$ and Tau_{P301L}). Our results show that TSPO increases appear before those of amyloid deposits. Moreover, the different parts of the hippocampus are differentially affected. Indeed, for both TSPO and amyloid, the subiculum is affected earlier and the ventral hippocampus later than the dorsal hippocampus. In the subiculum and the dorsal hippocampus of 3xTgAD mice, a positive correlation between TSPO and of amyloid deposit levels is observed. This data supports the hypothesis that TSPO could be used as a predictive marker of amyloid pathology. In addition, our immunohistochemical data shows a segregation of TSPO in the hippocampus and immunofluorescence imaging revealed a mainly microglial origin of the TSPO expression. Thus, imaging TSPO with CLINDE may be a good alternative to PET radiotracers.

1. Introduction

Alzheimer's disease (AD), the most common neurodegenerative disorder, is characterized by two neuropathological hallmark-lesions, the extracellular deposits of amyloid β (Aβ) and intracellular neurofibrillary tangles (NFT), formed by hyperphosphorylated tau proteins (P-Tau). Neuroinflammatory processes are also involved in the pathophysiology of AD even if their precise role with respect to the evolution of the pathology is debated (Calsolaro and Edison, 2016). Brain glial activation induces the overexpression of the 18kDa translocator protein (TSPO), which is therefore used as a neuroinflammatory marker. Several radiotracers were developed for *in vivo* imaging of TSPO by positron emission tomography (PET) or single-photon emission computed tomography (SPECT). In the field of AD research, some studies reported an increase in TSPO densities (Cagnin et al., 2001; Edison et al., 2008; Fan et al., 2015; Hamelin et al., 2016; Kreisl et al., 2013; Lyoo et al., 2015; Schuitemaker et al., 2013; Varrone et al., 2015; Versijpt et al., 2003) while others showed no effects (Golla et al., 2015; Gulyas et al., 2011; Schuitemaker et al., 2013; Varrone et al., 2013; Wiley et al., 2009). For a proper comparison of these clinical studies, it is important to highlight several methodological concerns. Some of these researches included participants with probable AD but medication, notably acetylcholinesterase inhibitors, which interfere with inflammatory pathways (Pohanka, 2014), was not always taken into account; measurement of the rs6971 TSPO polymorphism, which affects binding of high-affinity radiotracers (Owen et al., 2011) was not systematic, and, considerable age variability was observed between studies or in some cases between control and AD groups, which may be a confounding factor,

Abbreviations: TSPO, 18kDa translocator protein; SPECT, single-photon emission computed tomography

* Corresponding author at: Division of Adult Psychiatry, University Hospitals of Geneva, Chemin du Petit Bel-Air, 2, 1225 Geneva, Switzerland.
E-mail address: Philippe.millet@hcuge.ch (P. Millet).

https://doi.org/10.1016/j.nbd.2018.09.022
Received 18 May 2018; Received in revised form 3 September 2018; Accepted 23 September 2018
Available online 24 September 2018
0969-9961/

given the assumed effect of age on TSPO density (Cagnin et al., 2001; Gulyas et al., 2011) even if the latter is not always reported (Hamelin et al., 2016; Versijpt et al., 2003). In addition, depending on what quantification method is employed, the quantification of TSPO may be biased (Edison et al., 2008; Fan et al., 2015; Gulyas et al., 2011; Lyoo et al., 2015; Schuitemaker et al., 2013; Varrone et al., 2015). Indeed, some studies used the cerebellum as a reference (i.e. devoid of specific binding) or as a pseudo-reference region (i.e. assuming homogeneous amounts of TSPO between groups) (Golla et al., 2015; Gulyas et al., 2011; Hamelin et al., 2016; Kreisl et al., 2016; Lyoo et al., 2015; Versijpt et al., 2003; Wiley et al., 2009), which could possibly induce considerable bias given that other studies showed a trend (Cagnin et al., 2001) or a significant increase (Edison et al., 2008; Varrone et al., 2015) in TSPO in this brain region in AD patients. There were also intrinsic problems related to radiotracers, with more or less non-specific binding and sensitivity to the TSPO polymorphism (Owen et al., 2011). Unfortunately, all these constraints make it impossible to draw definitive conclusions on the involvement of the TSPO in AD. For example, it is still a matter of debate whether increases in TSPO are primary or secondary to AD-related neuropathology (Hamelin et al., 2016; Kreisl et al., 2013). However, knowing the timing of TSPO onset is important not only to the early detection of the disease but also to elucidate the presumed roles of TPSO. Indeed, TSPO could play a role in the pathophysiology of the disease and thus serve as a therapeutic target, as suggested by some studies (Barron et al., 2013; Szekely et al., 2004). The effects of TSPO may be neuroprotective or deleterious, as a function of the stage of neuropathology but also of the CNS cell type (Calsolaro and Edison, 2016; Ji et al., 2008). Given the complexity of the subject, efforts are still needed to identify other TSPO radiotracers with a more favorable quantification profile.

In parallel with clinical studies, TSPO density has been evaluated in simplified murine models carrying transgenes coding for mutated forms of human Tau, human APP alone or human APP in combination with human PS1. In the cerebellum, high specific binding of TSPO was reported in wild-type (WT) animals (Maeda et al., 2011). In addition, (APP/PS1) transgenic (Tg) animals showed an upward trend (Serriere et al., 2015), a significant increase (Rapic et al., 2013) or no changes (Mirzaei et al., 2016; Venneti et al., 2009) in TSPO binding in the cerebellum. However, the results of these studies converge on an increase in binding of TSPO radiotracers in the whole hippocampus of Tau Tg, APP Tg and (APP/PS1) Tg mice (James et al., 2015; Liu et al., 2015; Maeda et al., 2011; Mirzaei et al., 2016; Rapic et al., 2013; Serriere et al., 2015), which would occur before or after the occurrence of neuronal loss, in Tau and APP transgenic models, respectively (Maeda et al., 2011). Such a difference in the time of appearance of TSPO could be due to the fact that APP-only or Tau-only animal models are too simple and do not take into account the Tau-APP interactions occurring in human AD (Jagust, 2016; Wang et al., 2016). Indeed, several studies show that Aβ or Tau alone do not produce all AD pathological hallmarks, thus suggesting functional Tau-Aβ interactions (Delacourte et al., 2002; Musiek and Holtzman, 2015; Villemagne et al., 2015). In favor of this hypothesis, recent studies tend to show that, depending on the cerebral regions analyzed, Aβ may amplify Tau levels, Tau-induced neurodegeneration and the spreading of tauopathy (Johnson et al., 2016; Scholl et al., 2016; Wang et al., 2016). Even if Tau and Aβ play distinct roles in the disease, they could have aggravating effects on each other. Overall, using a rodent model combining APP and Tau should be more representative and informative of the links between inflammation, Tau- and Aβ-pathologies.

The aim of the present study was to investigate the efficacy of a TSPO radiotracer and to determine the time-course of the appearance of TSPO and amyloid deposits in a mouse model of AD combining amyloidosis and tauopathy. We used CLINDE, as this radiotracer has recently been shown to be effective in detecting the presence of TSPO-positive glioma cells in mice brain (Tsartsalis et al., 2015). The present experiments were conducted in the triple transgenic 3xTgAD mouse model (APP_{SWE}, $PS1_{M146V}$ and Tau_{P301L}) as it shows progressive Aβ- and tau-associated pathologies that resemble the temporal and regional development of AD in humans (Oddo et al., 2003a). First, we performed *in vitro* autoradiography experiments for TSPO (CLINDE) and amyloid deposits (DRM106) on serial sections of the hippocampus, one the "key" brain regions involved in AD. Then, we studied the localization of the TSPO signal in the hippocampus and its cellular origin using immunochemistry and double immunostaining, respectively. We also evaluated the use of CLINDE in *in vivo* and *ex vivo* experiments. Finally, as choroid plexus of mice showed elevated CLINDE binding, we explored if TSPO is expressed in human choroid plexus.

2. Materials and methods

2.1. Animals and human samples

Female triple transgenic (3xTgAD) heterozygote mice harboring the APP_{SWE}, $PS1_{M146V}$ and Tau_{P301L} transgenes and associated controls (C57B1/6J-Sv129) were housed in light-dark cycle LD12:12 with food and water provided *ad libitum*. Only females are used because of considerable sex differences in the progress of the pathology (Carroll et al., 2010; Hirata-Fukae et al., 2008) to augment homogeneity. All experimental procedures were approved by the Ethics Committee for Animal Experimentation of the Canton of Geneva, Switzerland. Human choroid plexus specimens come from authorized autopsies.

2.2. Immunochemistry

Four 21-months old 3xTgAD mice were transcardially perfused with 0.9% saline under 3% isoflurane anesthesia. Brains were removed, post-fixed (4% paraformaldehyde, 4°C, overnight) and cryoprotected (sucrose gradient, 5-20%, 48h). Brains were frozen in pre-cooled isopentane and transverse sections covering the rostro-caudal extent of the hippocampus, were cut on a cryostat and stored as free-floating slices (30 μm) in 1x PBS 0.05% azide.

Human choroid plexus (n = 8) were fixed in 15% formaldehyde solution for 3-4 weeks and then stored in 5% formaldehyde solution before embedding in paraffin. Sections (20 μm) were cut on a microtome in two series following by dewaxing and rehydrating.

Mice and human sections were washed twice 5 min with 1x PBS-0.2% Triton X-100 before overnight incubation with the primary antibody in 1x PBS-0.2% Triton X-100. After washing in PBS, the secondary antibody was added during 90 min followed by a revelation with 0.2 mg/ml DAB (Sigma-Aldrich) in 1x PBS, containing 100 μl/l H_2O_2. Free-floating slices were mounted onto gelatin-coated slides and stained in a cresyl violet solution. Choroid plexus treated with CD31 were also stained in a cresyl violet solution.

The following primary antibodies were used: mouse anti-β amyloid 4G8 (1/500, Biolegend, San Diego), mouse anti-phospho Tau (Ser202, Thr205) (AT8, 1/1000, ThermoFisher), goat anti-PBR (sc-23418, 1/200, Santa Cruz Biotechnology), mouse anti endothelial cell CD31 (M0823, 1/50, Dako) and rabbit anti-PBR (ab109497, 1/300, Abcam). Secondary antibodies used were rabbit anti-mouse HRP, anti-goat HRP or mice anti-rabbit HRP (1/200, Dako).

2.3. Double-immunofluorescence

Brain samples from 4 additional 3xTgAD mice (21 months) were treated for immunochemistry as described below. Slices (12 μm) were mounted onto gelatin-coated slides, washed twice 5 min with 1x PBS-0.2% Triton X-100 before 48 hours incubation with the anti-PBR antibody in 1x PBS-0.2% Triton X-100. After washing in PBS, the secondary antibody was added during 60 min. Then, after twice washing in PBS, the slices were incubated overnight with the anti-IBA1 or the anti-GFAP antibody in 1x PBS-0.2% Triton X-100. After washing in PBS, the secondary antibody was added during 60 min, slices were exposed to

Soudan black (0.3% in 70% ethanol) and then stained with DAPI (30 nM). The primary antibodies used were goat anti-PBR (sc-23418, 1/200, Santa Cruz Biotechnology), rabbit anti-ionized calcium-binding adapter molecule 1 (Iba1; 1/300, Wako) and rabbit anti-glial fibrillary acidic (Gfap; 1/500, Dako). The secondary antibodies were anti-rabbit Alexa 555-labeled and anti-goat Alexa 488-labeled. Images were observed using a fluorescent microscope (AxioPlan2, Zeiss) and acquired with the Axiovision software (Zeiss).

2.4. Radiotracers preparation

[^{125}I]-CLINDE was obtained by incubation (70°C, 20 min) of tributyltin precursor (100 μg) in acid acetic (100μl) with Na^{125}I (185-370 MBq, PerkinElmer) and peracetic acid (37%, 5μl). [^{125}I]-DRM106 was obtained by incubation (30 min) of tributyltin precursor (50 μg) in acetic acid (10μl) with 3M HCl (10μl), Na^{125}I (185-370 MBq, PerkinElmer) and hydrogen peroxide (30%, 1μl) (Chen et al., 2014). Reactions were then diluted in 50% acetonitrile (ACN) in water, injected onto a reversed-phase column (Bondclone C18) and [^{125}I]-CLINDE or [^{125}I]-DRM106 were isolated by a linear gradient HPLC run (5% to 95% ACN in 7mM H_3PO_4, 10 min). Radiochemical yield and purity were respectively above 60% and 98% for [^{125}I]-CLINDE and above 50% and 98% for [^{125}I]-DRM106. The specific activity was greater than 1000 GBq/μmol for [^{125}I]-CLINDE and 650 GBq/μmol for [^{125}I]-DRM106, based on the limit of detection of the ultraviolet absorbance and on the calibration curves established with cold reference compounds.

2.5. In vitro autoradiography

Mice (aged of 1-, 6-, 12- or 21-months) of both genotypes, WT and 3xTgAD (n = 4/age/genotype), were transcardially perfused with 0.9% saline under 3% isoflurane anesthesia. Brains were removed and frozen in pre-cooled isopentane. Transverse sections (20 μm), covering the rostro-caudal extent of the hippocampus, were cut on a cryostat and mounted as four series on gelatin-coated slides. Slices were first immersed in 1x PBS (30 min), then in radioactive buffer (90 min) and then rinsed twice in 4°C Tris-$MgCl_2$ buffer (3 min) and briefly washed in cold water. The radioactive buffer consists of Tris-$MgCl_2$ buffer (50 mM Tris HCl, 50 mM $MgCl_2$, pH 7.4) containing either [^{125}I]-CLINDE (0.11 MBq/ml) or [^{125}I]-DRM106 (0.11 MBq/ml) alone or in presence of 10 μM of unlabeled CLINDE or DRM106 to determine the non-specific binding. Slides were air-dried before exposure onto gamma-sensitive phosphor imaging plates (Fuji BAS-IP MS2325) for 30 min. Brain sections were then treated for acetylcholinesterase staining in order to delineate the region of interests (ROIs): antero-dorsal hippocampus, subiculum, dorsal hippocampus and ventral hippocampus.

Autoradiograms were analysed with the Fujifilm BAS-1800II phosphorimager using Aida Software V4.06 (Raytest Isotopenmessgerate GmbH) in presence of homemade ^{125}I calibration curves (see Supplemental data for details). Specific binding ratio (SBR) was calculated as follows: (Average radioactivity in ROI over at least 10 sections / radioactivity in ROI over 4 slices in the presence of 10 μM of unlabeled radiotracer) – 1. For each radiotracer, quantification was performed individually on the sub-regions of the hippocampus. For each animal, values in bilateral ROI were averaged.

2.6. SPECT and ex vivo imaging

Four 3xTgAD mice (aged of 21-months) performed a 60-min SPECT imaging with [^{125}I]-CLINDE. Animals were anesthetized with 3% isoflurane and placed in the U-SPECT-II imaging system (miLabs, Utrecht, Netherlands). Body temperature was maintained at 37 ± 1 °C using a thermostatically controlled heating blanket. Acquisition (60 frames of 84 sec) was initiated upon intravenous injection of the radiotracer (31.5 ± 1.42 MBq). SPECT tomograms were reconstructed with an ordered subsets expectation maximization (OSEM) algorithm using the HiSPECT software (SciVis GMBH, Göttingen, Germany). SPECT data were corrected for radioactive decay but not for attenuation, and scatter was applied. A factor analysis denosing was applied on dynamic images, as previously described (Tsartsalis et al., 2014; Tsartsalis et al., 2017). Summed SPECT images (10-60 min) were manually coregistered to a magnetic resonance imaging (MRI) atlas of the mouse brain using the PMOD software. Time activity curves (TACs) extracted from ROIs were normalized using the percentage of injected dose per cubic centimeter (%ID/cc). Immediately following scan acquisition, the anesthetized mice were euthanized, and their brains were frozen in pre-cooled isopentane (-20°C). Transverse sections (20 μm) were cut on a cryostat and exposed onto gamma-sensitive phosphor imaging plates (Fuji BAS-IP MS2325) overnight. Brain sections were then treated for acetylcholinesterase staining (Karnovsky and Roots, 1964). *Ex vivo* images were obtained using the Fujifilm BAS-1800II phosphorimager and Aida Software V4.06 (Raytest Isotopenmessgerate GmbH).

2.7. Specificity of the in vivo [^{125}I]-CLINDE signal

To determine the specificity of the [^{125}I]-CLINDE signal, we used SPECT examinations from a previous study whose aim was to detect TSPO in response to GL26 cell injections in the striatum (Tsartsalis et al., 2015). Eighty-two minutes after the injection of the radiotracer, 4 animals received 10 mg/kg of non-radioactive CLINDE. The total scan duration was 165 min. In the present study, we analyzed these brain scans in term of [^{125}I]-CLINDE accumulation/displacement in pituitary, ventricles and cerebellum. The percentage of the effect of unlabeled CLINDE injection was calculated as follow: (100 x %ID/cc in $ROI_{90\text{-}110\ min}$ / %ID/cc in $ROI_{60\text{-}80\ min}$)-100.

To determine the influence of the *in vivo* [^{125}I]-CLINDE accumulation in the choroid plexus on the signal measured in the hippocampus, an analysis of the CLINDE binding was conducted on the 4 mice used in the SPECT experiment and on 4 additional 3xTgAD mice (2 months, n = 2 and 12-months, n = 2) who also performed a 60-min SPECT imaging.

2.8. Red blood cell/plasma distribution

In heparinized blood samples (300 μl) from 3xTgAD and control mice (n = 2/genotype) 0.37 MBq of [^{125}I]-CLINDE was added for 15 min. Samples were centrifuged and radioactivity of both fractions of the whole blood (plasma and red blood cells) was counted using an automated γ-counter.

2.9. Statistics

Multivariate analysis of variance (MANOVA) was used to analyze the *in vitro* specific binding of [^{125}I]-CLINDE and [^{125}I]-DRM106 with genotype, age and hippocampal area as between subject factors. Repeated one-way ANOVA with ROI as between subject factor and time of measure as within subject factor was used to analyze the percentage of the effect of unlabeled CLINDE injection on [^{125}I]-CLINDE. When significant, analyses of variance were followed by group comparisons using the LSD *post hoc* test. Correlation analysis was performed with Pearson's correlation test. Data are presented as mean ± SEM. Sample size analysis with the graphical Douglas Altman's nomogram approach (Altman, 1991) was performed, and significant data was only reported if $p \leq 0.05$ and $\beta < 0.2$.

3. Results

3.1. In vitro quantification of TSPO and Amyloid

Representative [^{125}I]-CLINDE and [^{125}I]-DRM106 autoradiography images (for neuroinflammation and Aβ deposits, respectively) show

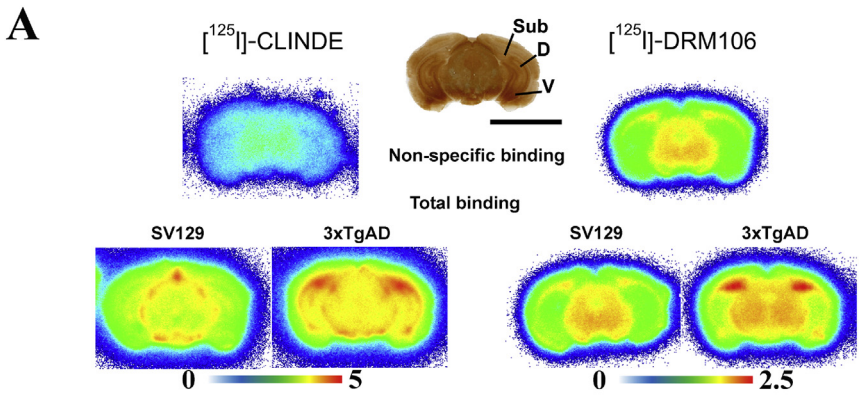

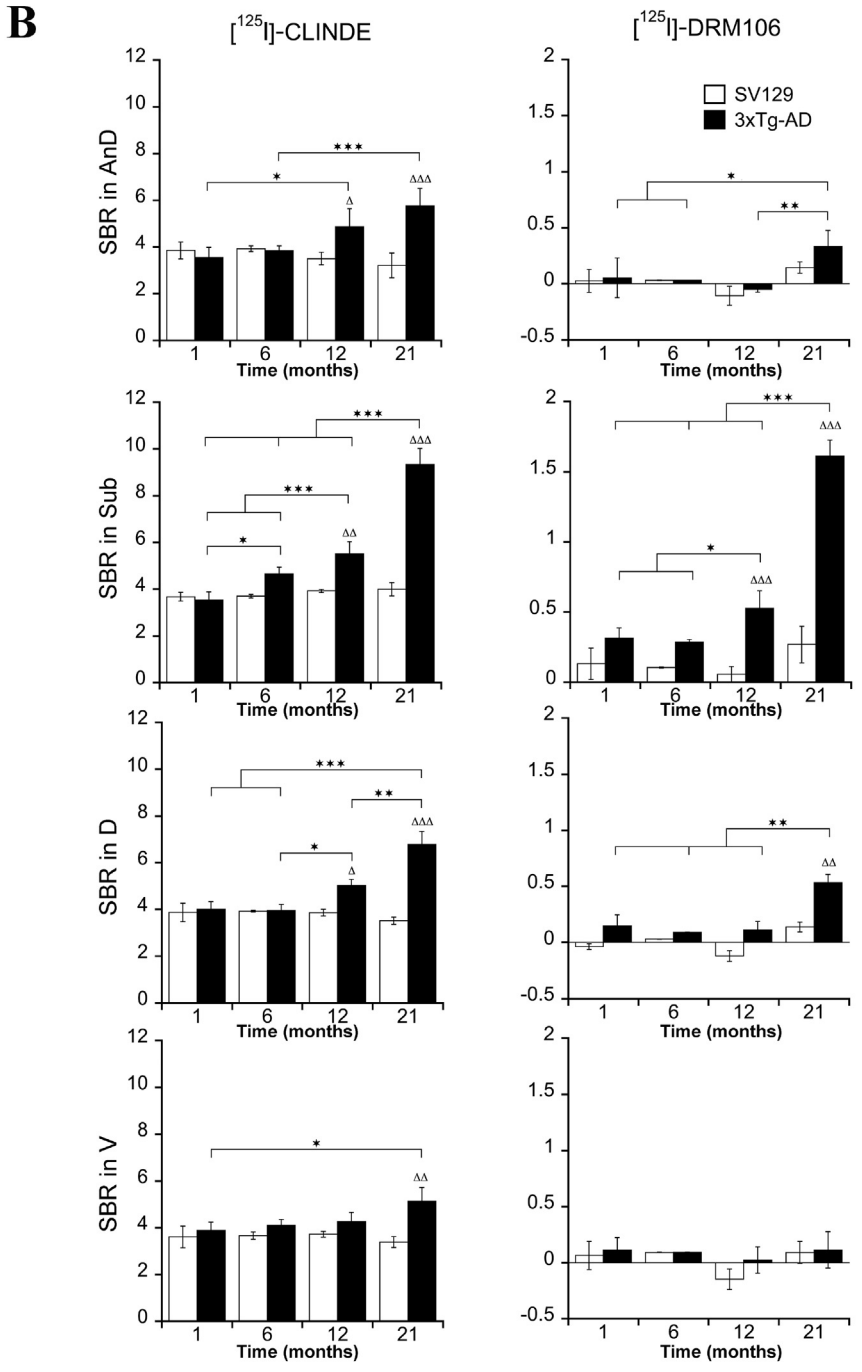

Fig. 1. *In vitro* quantification of [^{125}I]-CLINDE and [^{125}I]-DRM106 bindings in hippocampus of control and 3xTgAD mice.

(A) Acetylcholinesterase (left) is used to delineate the region of interests in the hippocampus: antero-dorsal (AnD), subiculum (Sub), dorsal (D) and ventral (V). Representative images of non-specific and total CLINDE and DRM bindings in 21-months old C57B1/6J-Sv129 mice (SV129) and in 21-months old 3xTgAD mice. CLINDE and DRM images were taken from the same individual. Color scale refers to activity in the autoradiograms (in MBq/mg). Scale bar: 500 µm. (B) The specific binding ratios (SBR) of [125I]-CLINDE (left column) and [125I]-DRM106 (right column) were calculated in antero-dorsal hippocampus (AnD), subiculum (Sub), dorsal hippocampus (D) and ventral hippocampus (V) in control (open bars) and 3xTgAD mice (closed bars) aged 1-, 6-, 12- and 21-months. Post-hoc tests indicate genotype differences at the same age (Δ) and age effects in 3xTgAD mice (★). The number of symbols indicates the significance level (1: $p < 0.05$; 2: $p < 0.01$; 3: $p < 0.001$). Data show mean ± SEM of 4 mice per genotype and per age.

high binding in the hippocampus of 3xTgAD compared to control mice (Fig. 1A). A visual radioactivity spatial gradient for both TSPO and Aβ deposits in the hippocampus was evident with the highest values in the subiculum and the lowest ones in the ventral hippocampus.

Bar graphs showing the specific binding ratios of [^{125}I]-CLINDE and [^{125}I]-DRM106 as a function of age, genotype and the hippocampal subdivision are depicted in Fig. 1B. The multivariate analysis of variance indicates main effects of genotype ($p < 0.001$), age ($p < 0.001$) and hippocampal area ($p < 0.001$) and, importantly, a significant genotype x age x hippocampal area interaction ($p < 0.001$).

For both targets and in all the hippocampal subdivisions, there was no age effect in control animals. In marked contrast, 3xTgAD mice were positive for both TSPO and amyloid deposits but the age effects on binding showed some specificities depending on the subdivision.

(1) In the antero-dorsal part of the hippocampus, an increase in TSPO binding is significant between the ages of 1- and 12-months ($p < 0.05$) and between the ages 6- and 21-months ($p < 0.001$). TSPO binding in 12- and 21-months old 3xTgAD mice was higher than their own controls ($p < 0.05$ and $p < 0.001$, respectively). In contrast, the only significant increase in β-amyloid deposits density is measured at 21-months as compared to the other age groups.
(2) In the subiculum, TSPO binding increased between the ages of 1- and 6-months ($p < 0.05$), between the ages of 6- and 12-months ($p < 0.001$) and between the ages of 12- and 21-months ($p < 0.001$). In addition, 12- and 21-months old 3xTgAD mice exhibited a higher TSPO density than their respective controls ($p < 0.01$ and $p < 0.001$, respectively). In addition, an increase in the [^{125}I]-DRM106 binding was observed between the ages of 6- and 12-months ($p < 0.05$) and a further elevation was observed between the ages of 12- and 21-months ($p < 0.001$). Moreover, 12- and 21-month old 3xTgAD mice exhibited more amyloid deposits than their respective controls ($p < 0.001$).
(3) In the dorsal hippocampus, an age effect was observed with an increase in TSPO binding between 6- and 12- months ($p < 0.05$) and between 12- and 21-months ($p < 0.01$). Twelve- and 21-months old 3xTgAD mice also showed elevated [^{125}I]-CLINDE binding as compared to their controls ($p < 0.05$ and $p < 0.001$, respectively). A significant increase in amyloid deposits is also observed in 21-months 3xTgAD mice in comparison to younger 3xTgAD mice ($p < 0.01$) and to their controls ($p < 0.01$).
(4) In the ventral hippocampus, the only statistically significant result is a higher TSPO availability in 21-months old 3xTgAD mice as compared to 1-month old ($p < 0.05$) and to their controls ($p < 0.01$).

In summary, TSPO over-expression was observed at 6-months old in subiculum, at 12-months old in the anterodorsal and dorsal hippocampus and at 21-months old in the ventral hippocampus. The presence of β-amyloid deposits is significant at the age of 12-months in subiculum, at the age of 21-months in the anterodorsal and dorsal hippocampus while no significant differences are observed in the ventral hippocampus at any age.

Post hoc analyses also indicated that in 21-months old 3xTgAD mice, the subiculum exhibited the highest level of TSPO followed by the dorsal parts of the hippocampus and finally the ventral hippocampus. Statistical analysis also indicated three levels of intensity of [^{125}I]-DRM106 binding in 21-months old 3xTgAD mice, as follows: subiculum > dorsal hippocampus > ventral and anterodorsal hippocampus.

Significant positive correlations between TSPO binding and Aβ deposits were observed in the subiculum and the dorsal hippocampus in 3xTgAD mice (Fig. 2). The relationship between TSPO and Aβ deposits is not significant in the anterodorsal or the ventral hippocampus (not shown).

3.2. Localization of TSPO-immunoreactivity in the hippocampus

To localize the areas of TSPO expression, immunochemistry against TSPO, P-Tau, and β amyloid was performed in 21-months old 3xTgAD mice (Fig. 3). The TSPO-immunoreactivity (TSPO-ir) showed its presence in the subiculum, in the radiatum layer and in the lacunosum moleculare of the dorsal and ventral hippocampus, respectively. Pyramidal cells are devoid of TSPO. Images showed P-Tau positive dystrophic neurites in subiculum, and cellular P-Tau-ir in pyramidal cells (stratum granulosum), mainly in the dorsal part of the hippocampus, as well as in some cells of the lacunosum moleculare of the hippocampus. Extracellular deposits of β amyloid were mainly observed in subiculum, but also, to a lesser extent, in the radiatum layer and beside the stratum granulosum. Intracellular β amyloid was observed in pyramidal cells as well as in the lacunosum moleculare of the hippocampus.

Therefore, the TSPO-ir localized in dorsal and ventral hippocampus, in areas close to intracellular and extracellular amyloid deposits, is not accompanied by P-Tau. In contrast, TSPO is also expressed in the subiculum where P-Tau positive dystrophic neurites and β amyloid deposits are present.

Regarding the cellular origin of the TSPO signal, representative results of double-labeling fluorescence with antibodies directed against TSPO and specific markers of microglia (IBA1) and astrocytes (GFAP) are shown in Fig. 4. In all hippocampal subdivisions, the main source of the TSPO-ir is microglia, as demonstrated by an important TSPO-IBA1 colocalization. In a much lesser extent, some TSPO-GFAP positive co-localizations are found, indicating that astrocytes are a minor source of TSPO in this experimental context.

3.3. SPECT imaging with [^{125}I]-CLINDE

Averaged [^{125}I]-CLINDE-SPECT images (10-60 min) in 21-month old 3xTgAD mice revealed the presence of TSPO in intra- and extracerebral regions (Fig. 5A-C). [^{125}I]-CLINDE binding is observed in pituitary, brain fissures, cerebellum, cortex, hippocampus and in ventricles containing choroid plexus. Corresponding time-activity curves in hippocampus, choroid plexus of lateral ventricles and pituitary are presented in Fig. 5D and showed an elevated [^{125}I]-CLINDE accumulation in pituitary and, to a lesser extent, in choroid plexus and hippocampus. The anatomical proximity of hippocampus with fissures and with third and lateral ventricles containing choroid plexus (see arrows in Fig. 5) suggests the presence of mutual spill-over effects that may distort the quantification of [^{125}I]-CLINDE in hippocampus. Indeed, the radioactivity measured in hippocampus is directly correlated with radioactivity in lateral ventricles ($r = 0.946$, $p < 0.001$). Therefore, to confirm the bias in radioactivity measured in choroid plexus and hippocampus produced by spill-over effects, a new SPECT imaging with [^{125}I]-CLINDE was performed in four younger additional mice. Considering the results of the eight mice, the positive correlation between hippocampus and lateral ventricles in term of [^{125}I]-CLINDE accumulation is highly significant ($r = 0.956$, $p < 0.001$; Fig 5.E). To determine if [^{125}I]-CLINDE accumulation in pituitary, lateral ventricles and cerebellum is specific, a displacement experiment of the *in vivo* [^{125}I]-CLINDE signal was performed in four wild-type mice. Unlabeled CLINDE induced a significant decrease in radioactivity in pituitary (-61 ± 3.9%, $p < 0.001$), lateral ventricles (-29.4 ± 7.6%, $p < 0.05$) and cerebellum (-36 ± 5.8%, $p < 0.05$), demonstrating some specificity of the signal in these areas.

To determine the free-fraction of circulating [^{125}I]-CLINDE, we measured the *in vitro* distribution of [^{125}I]-CLINDE in blood and found that 73.99 ± 11.24% of [^{125}I]-CLINDE was linked to red blood cells.

3.4. Ex vivo imaging with [^{125}I]-CLINDE

After the SPECT imaging procedure, the brains of the 21-months old 3xTgAD mice were processed for *ex vivo* imaging. In agreement with *in*

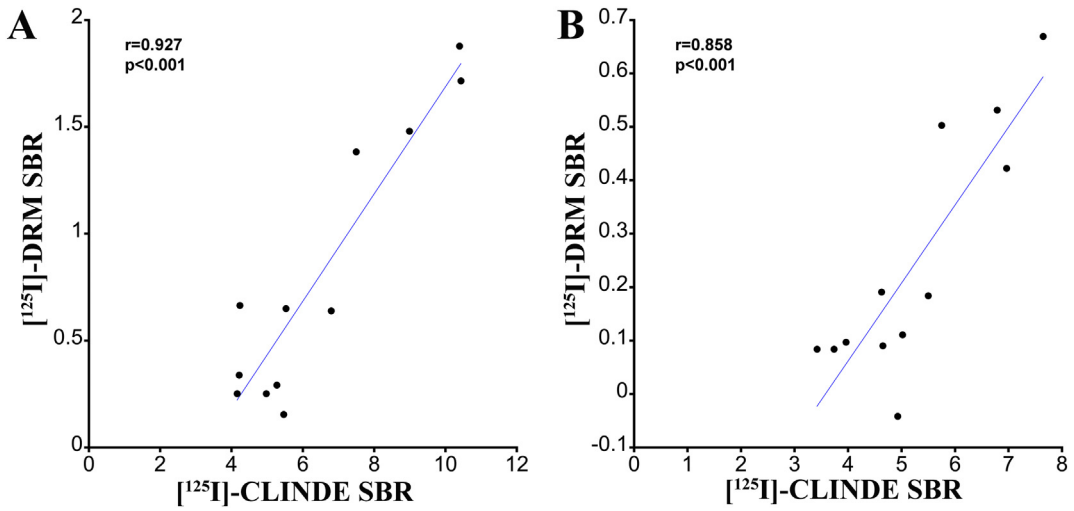

Fig. 2. Correlations between [^{125}I]-CLINDE and [^{125}I]-DRM106 bindings in the subiculum and the dorsal hippocampus of 3xTgAD mice.
Correlations of the specific binding ratios (SBR) of [125I]-CLINDE and [125I]-DRM106 in the subiculum (A) and the dorsal part of the hippocampus (B) in 6-, 12- and 21-months 3xTgAD mice. r = Spearman's correlation coefficient.

vivo observations, an intense signal was observed in third and lateral ventricles as well as in a ventral fissure and pituitary, which confirm the contamination of the endogenous signal in the hippocampus due to spill-over effects from adjacent regions (Fig. 5F).

3.5. TSPO expression in human choroid plexus

To determine if the TSPO expression in choroid plexus of mice is relevant for human studies, we performed immunochemistry against TSPO and CD31 in choroid plexus from eight subjects. As shown in the representative example in Fig. 6, both the epithelium and adjacent capillary (endothelial cells) of the choroid plexus are TSPO positive, in all subjects.

4. Discussion

This is the first study of TSPO imaging in a rodent model showing both Tau- and Aβ-pathology, and, the first to combine TSPO and amyloid imaging, as well as immunohistochemical localization, in different hippocampal subdivisions. We found that TSPO was mainly of microglial origin and was up-regulated before the appearance of Aβ deposits in all hippocampal areas. We also observed a positive correlation between TPSO and Aβ deposits in the subiculum and the dorsal hippocampus.

In the present study, we used [^{125}I]-CLINDE to determine if an age-related increase in neuroinflammation was present in 3xTgAD mice. *In vitro*, we reported effects of age and genotype on the distribution of [^{125}I]-CLINDE binding. In contrast to controls, 3xTgAD mice showed an increase in TSPO density, but importantly, the effect of the age was also dependent on the particular area of the hippocampus. Subiculum appears to be the first region affected by neuroinflammation, from the age of 6 months, while the increase in TSPO binding in the dorsal hippocampus was significant at 12 months and in ventral hippocampus only at 21 months. In parallel with TSPO, we showed an increase in binding of [^{125}I]-DRM106 which also depends on age and the particular hippocampal areas: in the subiculum an increase is evident at 12 months, in the dorsal hippocampus at 21 months, while in the ventral hippocampus no increase is observed at any age studied. [^{125}I]-DRM106 is present in the subiculum and the dorsal hippocampus where A4G8-immunoreactivity reveals the presence of amyloid plaques, but it is absent in the ventral hippocampus in which A4G8-immunoreactivity shows intracellular Aβ labeling. It is known that DRM106 is a preferential amyloid dense-cored neuritic plaque marker (Chen et al., 2015; Ji et al., 2015) and in light of these results, one may assume that DRM106 is not sensitive to intracellular Aβ and may not represent an early marker of amyloidosis. Nevertheless, intracellular Aβ is at least partly responsible for the formation of extracellular deposits (Oddo et al., 2006), indicates the presence of synaptic dysfunction (Oddo et al., 2003b) and exerts cytotoxic effects (Li et al., 2007), thus being a potentially valuable biomarker of early AD pathology. In this context, [^{125}I]-CLINDE might be of interest: indeed, its binding precedes that of [^{125}I]-DRM106 and is localized not only in regions where Aβ is found in the form of deposits but also in areas devoid of plaques but rich in intracellular Aβ. Indeed, despite the absence of amyloid plaques in the ventral hippocampus, we detected TSPO in this region (by means of autoradiography and immunochemistry). The early detection of activated microglia and astrocytes in (APP/PS1) Tg mice (Heneka et al., 2005) and postmortem human studies (Griffin et al., 1989; Rozemuller et al., 1989; Veerhuis et al., 2003) as compared to amyloid deposition or neurodegenerative alterations underlines the potential of TSPO as marker of early AD pathology. One possibility is that TSPO is induced by the presence of soluble Aβ in monomeric or polymeric state, thus, well before the appearance of the plaques. In agreement with this idea, Clarke and colleagues showed that injection of soluble Aβ forms induced neuroinflammation (Clarke et al., 2015) and Oddo et al. demonstrated that increase in intracellular Aβ preceded Aβ deposits in 3xTgAD mice (Oddo et al., 2003a; Oddo et al., 2003b). The results of our study are compatible with the hypothesis that the TSPO-dependent inflammation precedes the presence of amyloid plaques. In this context, future studies are warranted to specify whether causal links exist between increases in brain TSPO levels and the appearance of amyloid deposits. A recent study showing ameliorative effects on spatial memory and Aβ loads of transient administrations of PK11195 in 16-month old 3xTgAD female mice sustains the idea that TSPO is not only a marker of AD but also an actor of the progression of the pathology (Christensen and Pike, 2018).

Our study also shows that the time-course of the appearance of TSPO and amyloid deposits is not homogeneous across the hippocampus of 3xTgAD mice. The subiculum is the first hippocampal area affected by TSPO and Aβ deposits, displays the highest levels of both Aβ deposits and TSPO, and, is the only site of observation of dystrophic neurites. It is important to note that the subiculum plays an important role in the diffusion of Aβ (George et al., 2014). It is the hippocampal subregion showing atrophy and neuronal loss earlier than any other subregion in humans (Carlesimo et al., 2015; Mizutani and Kasahara, 1997). It is also in this subregion that atrophy and neuronal loss present

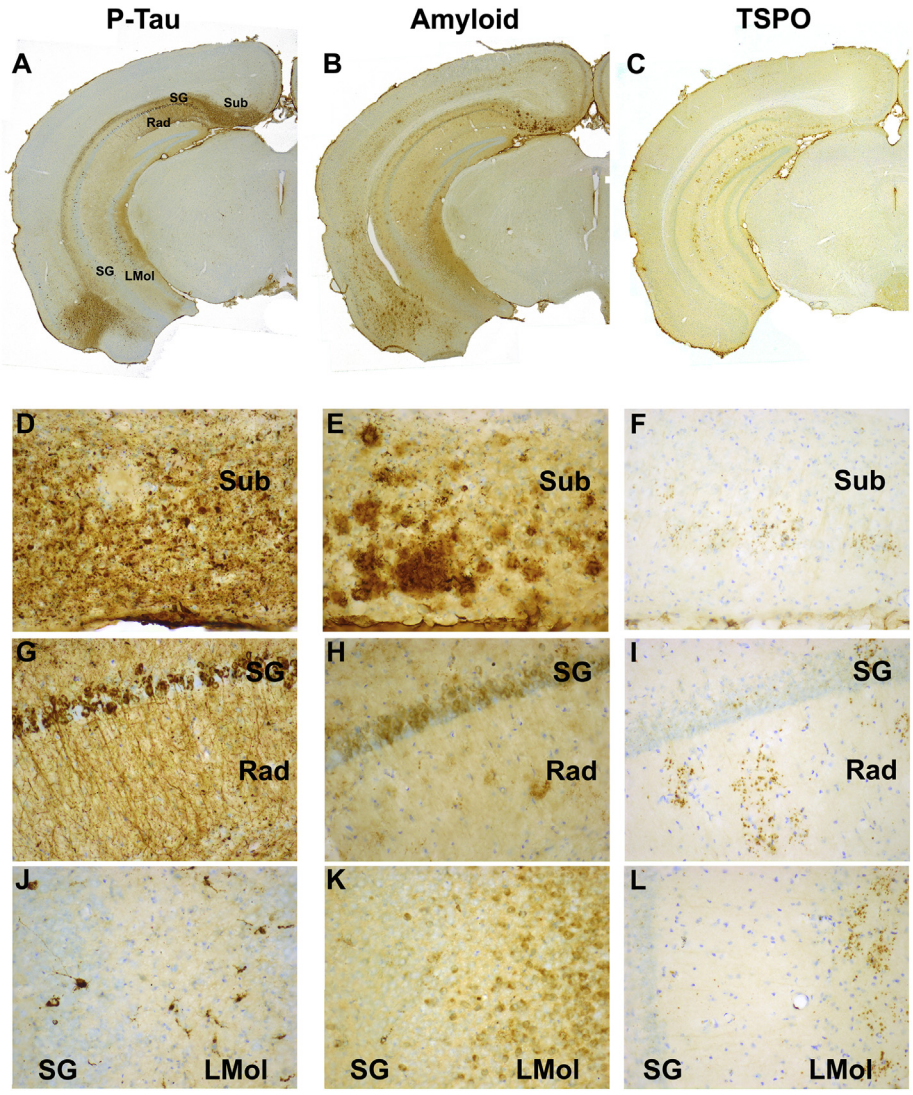

Fig. 3. Immunostaining of TSPO, ß amyloid, Phospho-Tau in the hippocampus of 3xTgAD mice.
(A-C) The first line shows immunostaining of AT8 (A; P-Tau), Aß4G8 (B; amyloid deposits) and PBR (C; TSPO) at a magnification of 2.5 x, in a representative hippocampal slice of 21 months-old 3xTgAD mice. (D-L) A magnification of 20 x was used to show details in subiculum (D-F), dorsal hippocampus (G-I) and ventral hippocampus (J-L) using AT8 (D, G, J), Aß4G8 (E, H, K) and PBR (F, I, L). LMol: lacunosum moleculare; Rad: radiatum layer; SG: stratum granulosum; Sub: subiculum. Scale bars: 100 µm (A-C) and 10 µm (D-L).

the greatest aggravation between the MCI state and AD (Carlesimo et al., 2015). These neurodegenerative phenomena also appear to be associated with cognitive decline (Hyman et al., 1990; Hyman et al., 1986). Overall, it will be important to evaluate whether the primacy of subicular inflammation in mice can extend to humans and if it would have a prognostic significance regarding the subsequent development of AD pathology. In favor of further studying TSPO as an early marker of AD, a close relationship between TSPO and amyloid (as shown by the correlation between CLINDE and DRM106 levels) is reported here, as it has been reported previously in a human AD study (Hamelin et al., 2016).

The cellular origin of TSPO expression in AD models also needs clarification. Since the physiological roles of astrocytes and microglia are considerably different, it would be important to know which cells over-express TSPO. In an APP Tg model, the TSPO is rather astrocytic whereas in a Tau Tg model, it is preferentially associated with microglia (Ji et al., 2008). In another study using double APP-PS1 Tg mice, TSPO was of microglial origin (Mirzaei et al., 2016). Post-mortem human studies suggest that TSPO is both astrocytic and microglial (Cosenza-Nashat et al., 2009; Venneti et al., 2009). The activation of both cell types in the disease has been demonstrated (Heneka et al., 2015; Ugbode et al., 2017). In the present report, we showed an elevated colocalization of TSPO with microglia and to a lesser degree some TSPO expression in astrocytes suggesting that TSPO may not exclusively have a microglial origin in 3xTgAD mice. Thus, 3xTgAD mice perhaps model to the human situation better than Tau Tg, APP Tg or (APP/PS1) Tg models, at least in terms of the TSPO-associated inflammation. It is also interesting to note that astrocytosis may be transient in familial AD but more persistent in the sporadic form of the disease (Rodriguez-Vieitez et al., 2016), which further complicates the understanding of the role of inflammation in AD. Further, besides the timing of activation of microglia in relation to amyloid pathology (Minett et al., 2016; Serrano-Pozo et al., 2011; Xiang et al., 2006; Zotova et al., 2013), the microglial response can be protective or deleterious for neurons (Mathys et al., 2017; Solito and Sastre, 2012). Therefore, further studies are still needed to fully understand the timing of astrocytic and microglial activation/inactivation in relation to TSPO and their possible neuroprotective or deleterious effects and the 3xTgAD model may be quite relevant in this context.

In the present study, *in vitro* autoradiography of [^{125}I]-CLINDE was

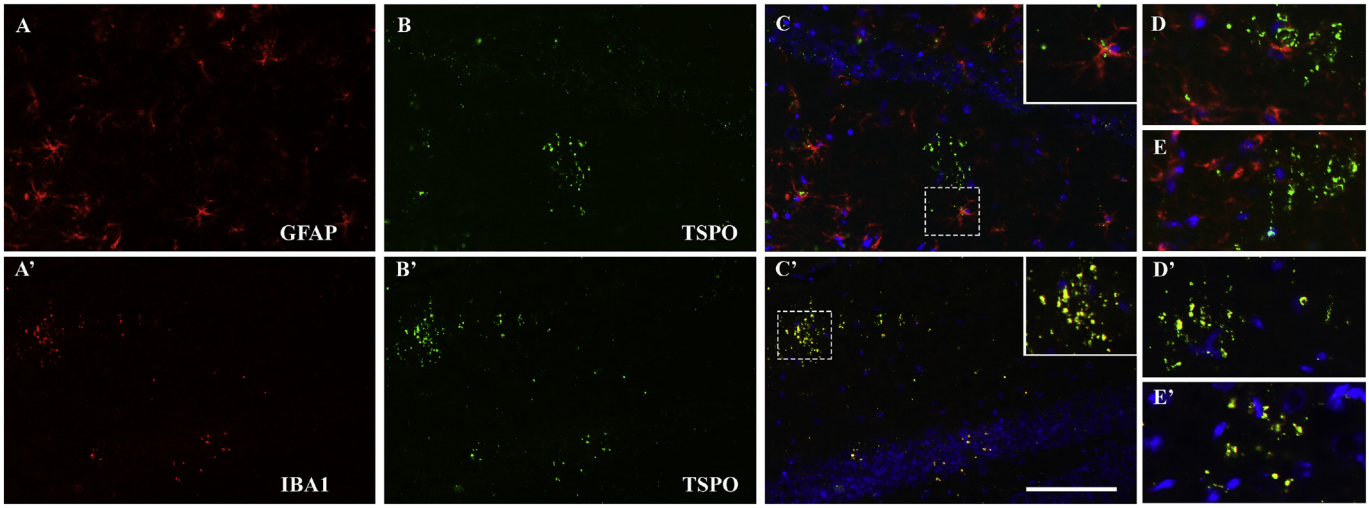

Fig. 4. Double-immunochemistry for TSPO in the hippocampus of 3xTgAD mice.
Double-immunofluorescence staining was performed using antibodies against GFAP (A) or IBAI (A') and TSPO (B, B'). Merge images show a weak relation between GFAP and TSPO (C-E) and a highly colocalization between TSPO and IBAI (C'-E') in dorsal hippocampus (C,C'), ventral hippocampus (D, D') and subiculum (E, E'). Nuclear staining (DAPI) is shown in blue. Scale bar: 50 μm (A-C, A'-C') and 100 μm (D-E, D'-E' and inserts).

also employed to validate the *in vivo* SPECT imaging and *ex vivo* observations. I*n vivo* quantification in hippocampus appears compromised. Firstly, we showed that the available free amounts of CLINDE in plasma of mice is low as shown by its high binding to red blood cells, in agreement with observations using other TSPO radiotracers (Canat et al., 1993; Di Grigoli et al., 2015; Turkheimer et al., 2007). Secondly, as the increase in TSPO in 3xTgAD brains appears to be a subtle and localized phenomenon, its detection by SPECT could be compromised by the detection limit of the SPECT camera and the partial volume effects. This idea is in accordance with previous AD studies (Janssen et al., 2016) and with others reporting high and quantifiable TSPO levels induced by exogenous manipulations (Mattner et al., 2011; Sridharan et al., 2017; Tsartsalis et al., 2015). Furthermore, as demonstrated by our in vivo displacement study, the TSPO signal in the cerebellum is, at least in part, specific. Thus, the cerebellum cannot be used as reference region for the determination of the non-specific binding. In agreement with a previous report showing an increase in the PK11195 signal in the cerebellum of Tg mice vs. controls (Rapic et al., 2013), cerebellum might also not represent a valid pseudo-reference region in animal models of AD. Finally, and certainly the most important constraint, high and specific fixation levels observed in areas close to hippocampus likely bias the radioactivity measurements in this region. The high levels of TPSO binding in pituitary that we report here, in accordance with a previous report (Kumar et al., 2012), may bias TSPO-measures in the ventral part of the hippocampus. Within the ventricles, the [^{125}I]-CLINDE binding most probably corresponds to a fixation to the choroid plexus (Cymerman et al., 1986; James et al., 2015; Kuhlmann and Guilarte, 2000; Turkheimer et al., 2007). The correlation of [^{125}I]-CLINDE signal between ventricles and hippocampus sustains the hypothesis that there is a considerable spill-over effect from choroid plexus to hippocampus, and vice versa. A human PET study has also reported the accumulation of PBR28, another TSPO radiotracer, in an area near the anterior and dorsal hippocampus, compatible with a localization in the choroid plexus (Hirvonen et al., 2012). In addition, we showed that TSPO is expressed in both epithelial and endothelial cells of the choroid plexus. Such an expression pattern suggests that TSPO in the choroid plexus may be unrelated to a neuroinflammatory reaction, thus further hampering the interpretation of TSPO alterations in adjacent brain regions, such as the hippocampus. The impact of the TSPO of choroid plexus could even become problematic in situations where morphological and functional alterations in the choroid plexus *per se* are observed, as in human AD (Krzyzanowska and Carro, 2012), and where the accumulation of the TSPO radiotracer is affected by age and genotype, as in the transgenic APP mice as compared to controls (James et al., 2015).

Therefore, even if the [^{125}I]-CLINDE signal is specific in the hippocampus, its *in vivo* detection and quantification in mice seem to be strongly influenced by the spill-over effect from choroid plexus and pituitary. On the contrary, this effect is probably much less important in human TSPO imaging, given the anatomical differences between rodent and human brain (Feng et al., 2017; Hirvonen et al., 2012).

A limitation of our current study lies on the intrinsic properties of *in vitro* autoradiography and immunohistochemistry: (i) In *in vitro* imaging, a percentage of the total binding is non-specific. This needs to be estimated and subtracted from the total binding, in order to estimate the specific binging. The non-specific binding may be directly measured using a displacement of the specific binding using a saturating concentration of unlabeled ligand (see paragraph 2.5 for details). In cases where the non-specific binding is high, as in the thalamus for [^{125}I]-DRM106 (see Fig. 1), it may be difficult to accurately measure the specific binding. Nevertheless, in the hippocampus, the region of interest in the present study, the non-specific binding was sufficiently low to allow accurate measurements of the specific binding. (ii) The use of antibodies is always subject to their degree of specificity. The A4G8 antibody has the ability to recognize the APP fragment in addition to Aβ. This cross-reactivity is not specific for A4G8 but is present on many other antibodies targeting amyloid peptides (6E10, 6F3D, BS85, BC05, BA27...) including those specific for the Aβ40 (MBC40) and Aβ42 (MBC42) fragments (Hunter and Brayne, 2017). However, beyond the issue of the specificity of the A4G8 antibody (and whether the intracellular labeling corresponds to APP or Aβ forms), we show in this study that the [^{125}I]-DRM106 does not bind on the intracellular forms of Aβ, confirming that this radiotracer is a preferential marker of Aβ deposits (Chen et al., 2015; Ji et al., 2015).

5. Conclusions

Our main results strongly suggest that TSPO-dependent inflammation precedes the onset of amyloid deposits in a murine model of AD. Furthermore, our results show that it is important to carry out the analyses in the sub-regions of the hippocampus and not in the structure in its entirety. *In vitro*, CLINDE allows a high segregation between control and triple (Tau/APP/PS1) transgenic individuals. The correlation between CLINDE and DRM106 suggests that increases in TSPO

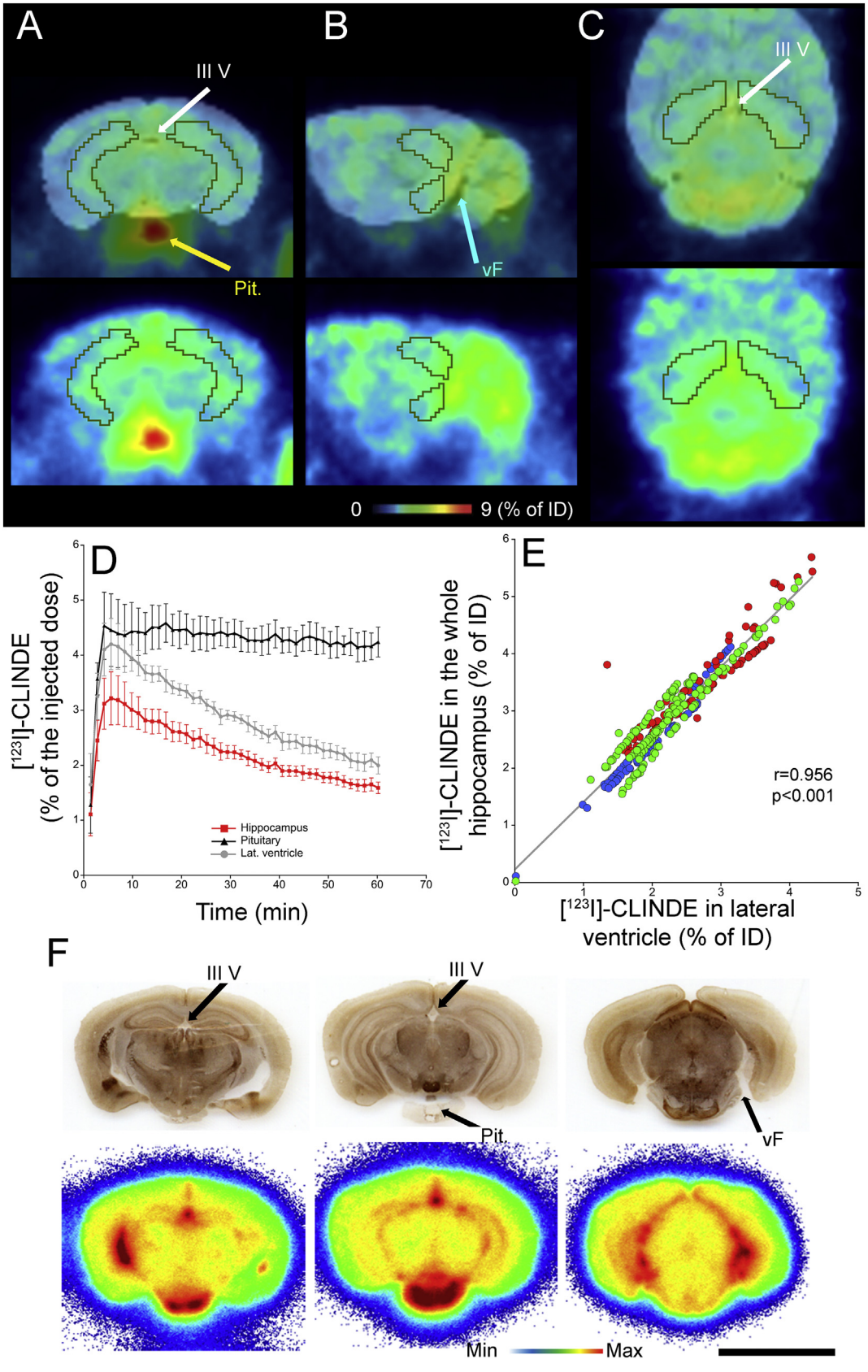

(caption on next page)

Fig. 5. *In vivo* and *ex vivo* imaging of [^{125}I]-CLINDE in 3xTgAD mice.
(A-C) Averaged image of four 3xTgAD mice (21 months) summed between 10 and 60 min post-[125I]-CLINDE injection. Coronal (A), sagittal (B) and axial planes (C) are presented with the mice hippocampus ROI provided in PMOD with (first line) or without (second line) the MRI image. Arrows indicate the third ventricle (III V), the pituitary (Pit.) and the ventral fissure (vF). Color scale refers to the % of the injected dose (ID). (D) In vivo TACs measured in hippocampus, pituitary and lateral (lat.) ventricle in 21-months old 3xTgAD mice. Data show mean ± SEM of 4 mice. (E) Correlation between [125I]-CLINDE in the whole hippocampus and the lateral ventricles (% of the injected dose, ID). Dots represent measures of [125I]-CLINDE at each time-point of the SPECT acquisition, in 2-months (n = 2, blue), 12-months (n = 2, red) and 21-months (n = 4, green) 3xTgAD mice. (F) Acetylcholinesterase (first line) and ex vivo images obtained from four 3xTgAD mice (21 months). In accordance with the Franklin and Paxinos atlas (Franklin and Paxinos, 2008), images were representative of different brain areas, as follows (distance from Bregma, mm: -2.06, -3.2 and -3.64). Color scale indicates the intensity of the signal. Arrows indicate the third ventricle (III V), the pituitary (Pit.) and the ventral fissure (vF). Scale bar: 500 μm.

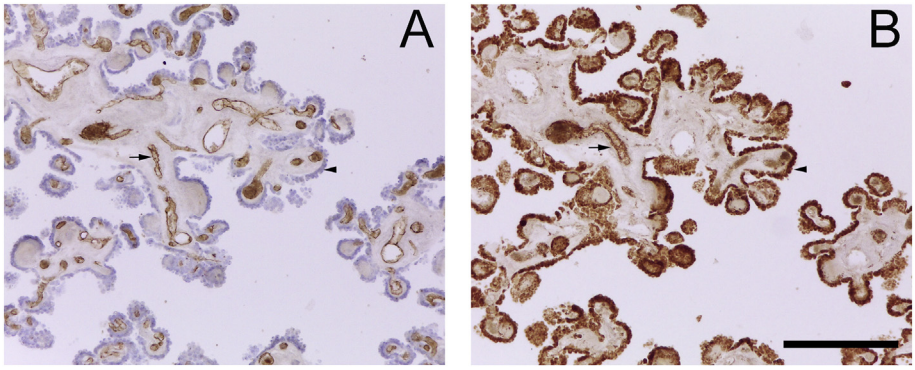

Fig. 6. TSPO-immunochemistry in human choroid plexus.
Immunostaining of CD31 (A; endothelial cells) and PBR (B; TSPO) in a representative choroid plexus of one subject. Sections treated with CD31 were counterstained with cresyl violet. The epithelium of the choroid plexus (indicated by arrow heads) is blue in A (CD31 negative) and brown in B (PBR positive). Some endothelial cells (indicated by arrows) are also PBR positive. Scale bar: 250 μm.

could be used as a predictive marker for the appearance of amyloid deposits. The *in vivo* use of CLINDE seems to be biased by the specific binding observed in adjacent structures that strongly express TSPO, such as choroid plexus and pituitary gland and the resulting partial volume effect. These technical drawbacks that are observed in small animal TSPO *in vivo* SPECT imaging with CLINDE, are probably much less important in human molecular imaging. Thus, in light of the results reported here, CLINDE could be of interest in the study of TSPO alterations in human pathologies.

Supplementary data to this article can be found online at https://doi.org/10.1016/j.nbd.2018.09.022.

Declaration of interest

The authors have no conflicts of interest to disclose.

Acknowledgments

The authors thank Frank M. Laferla, Salavatore Oddo and the University of California for providing the 3xTgAD mice that founded our own colony. This work was supported by the “Swiss Association for Alzheimer's Research” which was created in 2009 to finance Swiss fundamental and clinical research programs on Alzheimer's disease. Author S. Tsartsalis was supported by the Maria Zaousi Memorial Foundation (Greece) through a scholarship of the Hellenic State Scholarship Foundation. Author are grateful to Mrs. Maria Surini-Demiri and Mrs. Pascale Marin for their excellent technical assistance.

References

Altman, D.G., 1991. Practical Statistics for Medical Research. London, UK. Chapman & Hall.
Barron, A.M., et al., 2013. Ligand for translocator protein reverses pathology in a mouse model of Alzheimer's disease. J Neurosci. 33, 8891–8897.
Cagnin, A., et al., 2001. In-vivo measurement of activated microglia in dementia. Lancet. 358, 461–467.
Calsolaro, V., Edison, P., 2016. Neuroinflammation in Alzheimer's disease: Current evidence and future directions. Alzheimers Dement. 12, 719–732.
Canat, X., et al., 1993. Distribution profile and properties of peripheral-type benzodiazepine receptors on human hemopoietic cells. Life Sci. 52, 107–118.
Carlesimo, G.A., et al., 2015. Atrophy of presubiculum and subiculum is the earliest hippocampal anatomical marker of Alzheimer's disease. Alzheimers Dement (Amst). 1, 24–32.
Carroll, J.C., et al., 2010. Sex differences in beta-amyloid accumulation in 3xTg-AD mice: role of neonatal sex steroid hormone exposure. Brain Res. 1366, 233–245.
Chen, C.J., et al., 2014. Synthesis and biological evaluation of novel radioiodinated imidazopyridine derivatives for amyloid-beta imaging in Alzheimer's disease. Bioorg Med Chem. 22, 4189–4197.
Chen, C.J., et al., 2015. In vivo SPECT imaging of amyloid-beta deposition with radioiodinated imidazo[1,2-a]pyridine derivative DRM106 in a mouse model of Alzheimer's disease. J Nucl Med. 56, 120–126.
Christensen, A., Pike, C.J., 2018. TSPO ligand PK11195 improves Alzheimer-related outcomes in aged female 3xTg-AD mice. Neurosci Lett. 683, 7–12.
Clarke, J.R., et al., 2015. Alzheimer-associated Abeta oligomers impact the central nervous system to induce peripheral metabolic deregulation. EMBO Mol Med. 7, 190–210.
Cosenza-Nashat, M., et al., 2009. Expression of the translocator protein of 18 kDa by microglia, macrophages and astrocytes based on immunohistochemical localization in abnormal human brain. Neuropathol Appl Neurobiol. 35, 306–328.
Cymerman, U., et al., 1986. Evidence for species differences in 'peripheral' benzodiazepine receptors: an autoradiographic study. Neurosci Lett. 66, 153–158.
Delacourte, A., et al., 2002. Tau aggregation in the hippocampal formation: an ageing or a pathological process? Exp Gerontol. 37, 1291–1296.
Di Grigoli, G., et al., 2015. Radiosynthesis and Preliminary Biological Evaluation of [18F] VC701, a Radioligand for Translocator Protein. Mol Imaging. 14.
Edison, P., et al., 2008. Microglia, amyloid, and cognition in Alzheimer's disease: An [11C](R)PK11195-PET and [11C]PIB-PET study. Neurobiol Dis. 32, 412–419.
Fan, Z., et al., 2015. Influence of microglial activation on neuronal function in Alzheimer's and Parkinson's disease dementia. Alzheimers Dement. 11 e7, 608–621.
Feng, L., et al., 2017. The Variability of Translocator Protein Signal in Brain and Blood of Genotyped Healthy Humans Using In Vivo 123I-CLINDE SPECT Imaging: A Test-Retest Study. J Nucl Med. 58, 989–995.
Franklin, K.B.J., Paxinos, G., 2008. The mouse brain in stereotaxic coordinates, 3th ed. Elsevier Academic, London.
George, S., et al., 2014. Lesion of the subiculum reduces the spread of amyloid beta pathology to interconnected brain regions in a mouse model of Alzheimer's disease. Acta Neuropathol Commun. 2, 17.
Golla, S.S., et al., 2015. Quantification of [18F]DPA-714 binding in the human brain: initial studies in healthy controls and Alzheimer's disease patients. J Cereb Blood Flow Metab. 35, 766–772.
Griffin, W.S., et al., 1989. Brain interleukin 1 and S-100 immunoreactivity are elevated in Down syndrome and Alzheimer disease. Proc Natl Acad Sci U S A. 86, 7611–7615.
Gulyas, B., et al., 2011. Age and disease related changes in the translocator protein (TSPO) system in the human brain: positron emission tomography measurements with [11C]vinpocetine. Neuroimage. 56, 1111–1121.
Hamelin, L., et al., 2016. Early and protective microglial activation in Alzheimer's disease: a prospective study using 18F-DPA-714 PET imaging. Brain. 139, 1252–1264.
Heneka, M.T., et al., 2005. Focal glial activation coincides with increased BACE1 activation and precedes amyloid plaque deposition in APP[V717I] transgenic mice. J Neuroinflammation. 2, 22.
Heneka, M.T., et al., 2015. Neuroinflammation in Alzheimer's disease. Lancet Neurol. 14, 388–405.
Hirata-Fukae, C., et al., 2008. Females exhibit more extensive amyloid, but not tau, pathology in an Alzheimer transgenic model. Brain Res. 1216, 92–103.
Hirvonen, J., et al., 2012. Increased in vivo expression of an inflammatory marker in

temporal lobe epilepsy. J Nucl Med. 53, 234–240.
Hunter, S., Brayne, C., 2017. Do anti-amyloid beta protein antibody cross reactivities confound Alzheimer disease research? J Negat Results Biomed. 16 (1).
Hyman, B.T., et al., 1986. Perforant pathway changes and the memory impairment of Alzheimer's disease. Ann Neurol. 20, 472–481.
Hyman, B.T., et al., 1990. Memory-related neural systems in Alzheimer's disease: an anatomic study. Neurology. 40, 1721–1730.
Jagust, W., 2016. Tau and beta-Amyloid-The Malignant Duo. JAMA Neurol. 73, 1049–1050.
James, M.L., et al., 2015. PET imaging of translocator protein (18 kDa) in a mouse model of Alzheimer's disease using N-(2,5-dimethoxybenzyl)-2-18F-fluoro-N-(2-phenoxyphenyl)acetamide. J Nucl Med. 56, 311–316.
Janssen, B., et al., 2016. Imaging of neuroinflammation in Alzheimer's disease, multiple sclerosis and stroke: Recent developments in positron emission tomography. Biochim Biophys Acta. 1862, 425–441.
Ji, B., et al., 2008. Imaging of peripheral benzodiazepine receptor expression as biomarkers of detrimental versus beneficial glial responses in mouse models of Alzheimer's and other CNS pathologies. J Neurosci. 28, 12255–12267.
Ji, B., et al., 2015. Distinct binding of amyloid imaging ligands to unique amyloid-beta deposited in the presubiculum of Alzheimer's disease. J Neurochem. 135, 859–866.
Johnson, K.A., et al., 2016. Tau positron emission tomographic imaging in aging and early Alzheimer disease. Ann Neurol. 79, 110–119.
Karnovsky, M.J., Roots, L., 1964. A "Direct-Coloring" Thiocholine Method for Cholinesterases. J Histochem Cytochem. 12, 219–221.
Kreisl, W.C., et al., 2013. In vivo radioligand binding to translocator protein correlates with severity of Alzheimer's disease. Brain. 136, 2228–2238.
Kreisl, W.C., et al., 2016. (11)C-PBR28 binding to translocator protein increases with progression of Alzheimer's disease. Neurobiol Aging. 44, 53–61.
Krzyzanowska, A., Carro, E., 2012. Pathological alteration in the choroid plexus of Alzheimer's disease: implication for new therapy approaches. Front Pharmacol. 3, 75.
Kuhlmann, A.C., Guilarte, T.R., 2000. Cellular and subcellular localization of peripheral benzodiazepine receptors after trimethyltin neurotoxicity. J Neurochem. 74, 1694–1704.
Kumar, A., et al., 2012. Evaluation of age-related changes in translocator protein (TSPO) in human brain using (11)C-[R]-PK11195 PET. J Neuroinflammation. 9, 232.
Li, M., et al., 2007. The role of intracellular amyloid beta in Alzheimer's disease. Prog Neurobiol. 83, 131–139.
Liu, B., et al., 2015. In Vivo Detection of Age- and Disease-Related Increases in Neuroinflammation by 18F-GE180 TSPO MicroPET Imaging in Wild-Type and Alzheimer's Transgenic Mice. J Neurosci. 35, 15716–15730.
Lyoo, C.H., et al., 2015. Cerebellum Can Serve As a Pseudo-Reference Region in Alzheimer Disease to Detect Neuroinflammation Measured with PET Radioligand Binding to Translocator Protein. J Nucl Med. 56, 701–706.
Maeda, J., et al., 2011. In vivo positron emission tomographic imaging of glial responses to amyloid-beta and tau pathologies in mouse models of Alzheimer's disease and related disorders. J Neurosci. 31, 4720–4730.
Mathys, H., et al., 2017. Temporal Tracking of Microglia Activation in Neurodegeneration at Single-Cell Resolution. Cell Rep. 21, 366–380.
Mattner, F., et al., 2011. Evaluation of [(1)(2)(3)I]-CLINDE as a potent SPECT radiotracer to assess the degree of astroglia activation in cuprizone-induced neuroinflammation. Eur J Nucl Med Mol Imaging. 38, 1516–1528.
Minett, T., et al., 2016. Microglial immunophenotype in dementia with Alzheimer's pathology. J Neuroinflammation. 13, 135.
Mirzaei, N., et al., 2016. In vivo imaging of microglial activation by positron emission tomography with [(11)C]PBR28 in the 5XFAD model of Alzheimer's disease. Glia. 64, 993–1006.
Mizutani, T., Kasahara, M., 1997. Hippocampal atrophy secondary to entorhinal cortical degeneration in Alzheimer-type dementia. Neurosci Lett. 222, 119–122.
Musiek, E.S., Holtzman, D.M., 2015. Three dimensions of the amyloid hypothesis: time, space and 'wingmen'. Nat Neurosci. 18, 800–806.
Oddo, S., et al., 2003a. Amyloid deposition precedes tangle formation in a triple transgenic model of Alzheimer's disease. Neurobiol Aging. 24, 1063–1070.
Oddo, S., et al., 2003b. Triple-transgenic model of Alzheimer's disease with plaques and tangles: intracellular Abeta and synaptic dysfunction. Neuron. 39, 409–421.
Oddo, S., et al., 2006. A dynamic relationship between intracellular and extracellular pools of Abeta. Am J Pathol. 168, 184–194.
Owen, D.R., et al., 2011. Mixed-affinity binding in humans with 18-kDa translocator protein ligands. J Nucl Med. 52, 24–32.
Pohanka, M., 2014. Inhibitors of acetylcholinesterase and butyrylcholinesterase meet immunity. Int J Mol Sci. 15, 9809–9825.
Rapic, S., et al., 2013. Imaging microglial activation and glucose consumption in a mouse model of Alzheimer's disease. Neurobiol Aging. 34, 351–354.
Rodriguez-Vieitez, E., et al., 2016. Diverging longitudinal changes in astrocytosis and amyloid PET in autosomal dominant Alzheimer's disease. Brain. 139, 922–936.
Rozemuller, J.M., et al., 1989. Microglial cells around amyloid plaques in Alzheimer's disease express leucocyte adhesion molecules of the LFA-1 family. Neurosci Lett. 101, 288–292.
Scholl, M., et al., 2016. PET Imaging of Tau Deposition in the Aging Human Brain. Neuron. 89, 971–982.
Schuitemaker, A., et al., 2013. Microglial activation in Alzheimer's disease: an (R)-[(1)(1)C]PK11195 positron emission tomography study. Neurobiol Aging. 34, 128–136.
Serrano-Pozo, A., et al., 2011. Reactive glia not only associates with plaques but also parallels tangles in Alzheimer's disease. Am J Pathol. 179, 1373–1384.
Serriere, S., et al., 2015. Amyloid load and translocator protein 18 kDa in APPswePS1-dE9 mice: a longitudinal study. Neurobiol Aging. 36, 1639–1652.
Solito, E., Sastre, M., 2012. Microglia function in Alzheimer's disease. Front Pharmacol. 3, 14.
Sridharan, S., et al., 2017. Comparative Evaluation of Three TSPO PET Radiotracers in a LPS-Induced Model of Mild Neuroinflammation in Rats. Mol Imaging Biol. 19, 77–89.
Szekely, C.A., et al., 2004. Nonsteroidal anti-inflammatory drugs for the prevention of Alzheimer's disease: a systematic review. Neuroepidemiology. 23, 159–169.
Tsartsalis, S., et al., 2014. Quantification of GABAA receptors in the rat brain with [(123)I]Iomazenil SPECT from factor analysis-denoised images. Nucl Med Biol. 41, 186–195.
Tsartsalis, S., et al., 2015. SPECT imaging of glioma with radioiodinated CLINDE: evidence from a mouse GL26 glioma model. EJNMMI Res. 5, 9.
Tsartsalis, S., et al., 2017. A single-scan protocol for absolute D2/3 receptor quantification with [123I]IBZM SPECT. Neuroimage. 147, 461–472.
Turkheimer, F.E., et al., 2007. Reference and target region modeling of [11C]-(R)-PK11195 brain studies. J Nucl Med. 48, 158–167.
Ugbode, C., et al., 2017. Astrocytic transporters in Alzheimer's disease. Biochem J. 474, 333–355.
Varrone, A., et al., 2013. In vivo imaging of the 18-kDa translocator protein (TSPO) with [18F]FEDAA1106 and PET does not show increased binding in Alzheimer's disease patients. Eur J Nucl Med Mol Imaging. 40, 921–931.
Varrone, A., et al., 2015. Positron emission tomography imaging of the 18-kDa translocator protein (TSPO) with [18F]FEMPA in Alzheimer's disease patients and control subjects. Eur J Nucl Med Mol Imaging. 42, 438–446.
Veerhuis, R., et al., 2003. Amyloid beta plaque-associated proteins C1q and SAP enhance the Abeta1-42 peptide-induced cytokine secretion by adult human microglia in vitro. Acta Neuropathol. 105, 135–144.
Venneti, S., et al., 2009. PK11195 labels activated microglia in Alzheimer's disease and in vivo in a mouse model using PET. Neurobiol Aging. 30, 1217–1226.
Versijpt, J.J., et al., 2003. Assessment of neuroinflammation and microglial activation in Alzheimer's disease with radiolabelled PK11195 and single photon emission computed tomography. A pilot study. Eur Neurol. 50, 39–47.
Villemagne, V.L., et al., 2015. Tau imaging: early progress and future directions. Lancet Neurol. 14, 114–124.
Wang, L., et al., 2016. Evaluation of Tau Imaging in Staging Alzheimer Disease and Revealing Interactions Between beta-Amyloid and Tauopathy. JAMA Neurol. 73, 1070–1077.
Wiley, C.A., et al., 2009. Carbon 11-labeled Pittsburgh Compound B and carbon 11-labeled (R)-PK11195 positron emission tomographic imaging in Alzheimer disease. Arch Neurol. 66, 60–67.
Xiang, Z., et al., 2006. Microglia activation in the brain as inflammatory biomarker of Alzheimer's disease neuropathology and clinical dementia. Dis Markers. 22, 95–102.
Zotova, E., et al., 2013. Inflammatory components in human Alzheimer's disease and after active amyloid-beta42 immunization. Brain. 136, 2677–2696.